Microstructure and Crystallography of α Phase Nucleated Dynamically during Thermo-Mechanical Treatments in Metastable β Titanium Alloy

Jiangkun Fan, Jinshan Li, Yudong Zhang, Hongchao Kou, Lionel Germain, Nathalie Siredey-Schwaller, Claude Esling

Microstructure and Crystallography of α Phase Nucleated Dynamically during Thermo-Mechanical Treatments in Metastable β Titanium Alloy**

By *Jiangkun Fan,* Jinshan Li, Yudong Zhang, Hongchao Kou, Lionel Germain, Nathalie Siredey-Schwaller* and *Claude Esling*

The α phase nucleated dynamically during the thermo–mechanical coupling process in titanium alloy is really interesting but difficult to sufficiently ascertain. In the present work, the α phase nucleation behavior, the orientation relationship between α/β as well as the phase transformation kinetics during hot deformation of Ti-5553 alloy were investigated in-depth. Results reveal that the "necklace" microstructure formed. The Burgers orientation relationship between α/β phases has been destroyed gradually. The β → α phase transformation is obviously retarded during the hot compression due to the competitive effect of softening process (dynamic recovery/recrystallization). These results could provide valuable reference for process optimization and the microstructural evolution controlling.

1. Introduction

Metastable β titanium alloys, such as Ti–10V–2Fe–3Al (Ti–1023), Ti–5Al–5Mo–5V–1Cr–1Fe (VT22), and Ti–5Al–5Mo–5V–3Cr (Ti–5553), are increasingly employed in the aerospace industry because of their higher yield strength, better hardenability, better fatigue, and crack propagation properties than α + β titanium alloys.[1,2] Microstructural development in these alloys depends on the processing parameters, such as the type of thermo-mechanical process, temperature, strain, strain rates, and cooling rates. Moreover, metastable β titanium alloys are usually sensitive to process parameters, even during isothermal processing.[3] Hence, significant effort to understand the microstructural evolution of metastable β titanium alloys related to thermo-mechanical process have been done in the past decade.[4–7]

The β → α phase transformation happens during the thermo-mechanical processing below the β transus temperature (T_β). Generally, heterogeneous nucleation mechanisms include grain boundary nucleation, dislocation nucleation, and vacancy nucleation. Although much more defects are introduced in microstructure during deformation, the α precipitates nucleated mainly at the interface of two adjacent β grains, triple junctions or quadruple points of β grains. The reasons could be summarized as the following aspects: (i) the higher interface energy could decrease the critical nucleation energy; (ii) only part of interface of second phase need to be reconstructed; (iii) the composition segregation is more significant at the grain boundaries (GBs). In Ti–5553 alloy, the dominant microstructural evolution mechanism during hot deformation close to the T_β is dynamic recovery (DRV) of the β phase,[6,8] with a certain degree of the dynamic recrystallization (DRX).[9] The α precipitates might nucleate at these GBs preferentially including high angle grain boundaries (HAGBs) and low angle grain boundaries (LAGBs). Hence, dynamic stress induced phase transformations (DSIPT) might happen during the thermo-mechanical processing due to the more nucleation sites and accelerating

[*] *Dr. J. Fan, Prof. J. Li, Prof. H. Kou*
State Key Laboratory of Solidification Processing, Northwestern Polytechnical University, Xi'an 710072, P.R. China
E-mail: fjk2006ok@163.com
Dr. J. Fan, Dr. Y. Zhang, Dr. L. Germain, Dr. N. Siredey-Schwaller, Prof. C. Esling
Laboratoire d'Étude des Microstructures et de Mécanique des Matériaux (LEM3), CNRS 7239, Université de Lorraine, 57045 Metz, France
Dr. J. Fan, Dr. Y. Zhang, Dr. L. Germain, Dr. N. Siredey-Schwaller, Prof. C. Esling
Laboratory of Excellence on Design of Alloy Metals for low-mAss Structures (DAMAS), Université de Lorraine, 57045 Metz, France

[**] *This work was supported by the National Natural Science Foundation of China (No. 51371143), Programme PHC Cai Yuanpei (No. 30249RD) and Major State Research Development Program of China (2016YFB0701303).*

growth of α precipitates.[10] Some other researches also implied a competitive relationship between precipitation and recrystallization.[11,12] Unfortunately, except earlier studies of martensite-based strain induced transformation following cold deformation,[13] the DSIPT about β ↔ α phase transformation in titanium alloys does not seem to have been fully assessed and exploited.

In general, the transformation from prior body-centered cubic (BCC) β phase to hexagonal close-packed (HCP) α phase respects the Burgers orientation relationship (BOR)[14]: $\{0001\}_\alpha // \{110\}_\beta, \langle 11\bar{2}0\rangle_\alpha // <111>_\beta$, and possess a low-energy, semi-coherent interface.[15] The BOR has a significant effect on texture inheritance and crystallographic α variant selection during the $\alpha \rightarrow \beta \rightarrow \alpha$ phase transformation.[16–18] At the beginning of deformation, dislocations are likely able to cross the semi-coherent interphase boundaries.[19] During further straining, however, the coherency of the interfaces is reduced due to the interaction of the boundaries with lattice dislocations.[20] The transition of the semi-coherent interfaces into incoherent ones can also accelerate, significantly, the spheroidization of the lamellar microstructure.[21] The study by He et al.[22] indicated that external factors (strain, strain rate, and cooling rate) have a slight influence on the obeying of BOR during $\beta \rightarrow \alpha$ phase transformation. But others scientists have found that the average deviation from the BOR reaches a value of 34.5° at a strain of 1.2 in Ti–5Al–5Mo–5V–1Cr–1Fe.[23] The deviation would also increase with the deformation strain. Furthermore, hot deformation could give a significant effect on the morphology of the subsequently precipitated α phase.[10]

The aforementioned investigations are useful for understanding microstructural evolution of metastable β titanium alloys during hot deformation. However, a clear understanding about the characteristics of the dynamic α precipitation during deformation is still not entirely available, and even be ignored. The main reasons are: (i) the microstructure evolution under the thermal field and force field simultaneously would be more complicated; (ii) the large quantity of crystal defects (dislocation, stacking fault, slip band, etc.) induced by deformation and dynamic softening (DRV/DRX) may be interact with dynamic $\beta \rightarrow \alpha$ phase transformation. Therefore, the objective of the present work, therefore, focuses on dynamic $\beta \rightarrow \alpha$ phase transformation of Ti–5553 alloy during the thermo-mechanical processing. The α precipitation mechanism, orientation relationship between α/β, substructures formed during deformation, as well as the effect of deformation on the kinetics of $\beta \rightarrow \alpha$ phase transformation were examined and discussed in this work. The results of the present work are expected to provide valuable reference for process optimization and the microstructural evolution control.

2. Materials and Methods

The as-received material was an (α + β) forged Ti–5553 bar with chemical composition (wt%) of Al: 5.26; Mo: 4.99; V: 4.80; Cr: 2.86; Fe: 0.42; Ti: balance. The β transus temperature determined by metallographic observations is approximately 870 °C.

Cylindrical specimens, 10 mm in diameter and 15 mm in height, were machined from the forged bar. They were then solution treated at 900 °C for 30 min followed by water quenching, in order to obtain single β phase state with homogeneous microstructure and free from residual stress induced by forging. Hot compression tests (temperature 800 °C, two strain rates 0.0005 s^{-1} and 0.001 s^{-1}, two true strains 0.7 and 1.2) were conducted in a Gleeble-3500 thermo-mechanical simulator with the compression direction along the cylindrical axis of the specimens. Prior to compression, each specimen was heated to the processing temperatures at a rate of 25 °C s^{-1} and then held for 10 s before the compression to ensure an establishment of a homogeneous temperature in the specimen. The temperature was controlled by a thermocouple welded to the central part of the specimen surface. Graphite lubrication was applied to the anvil and the specimen, in order to reduce the relative friction between the two parts to enhance deformation homogeneity and also to prevent adhesion. After compression, all specimens were immediately quenched in water in order to retain the deformed microstructures. For comparison, the specimens corresponding to all hot-compression were heat treated under exactly the same thermal conditions (heating, isothermal holding and cooling), but without any deformation.

The heat treated and the hot deformed specimens were sectioned along their cylindrical axis. For the optical microstructure examinations, the specimens were first mechanically polished and then etched in a modified Kroll's reagent of 10 Vol% HF, 10 Vol% HNO_3, and 80 Vol% H_2O for 15 s. Microstructural examinations were conducted using an OLYMPUS/PMG3 optical microscope. Quantitative measurements of α phase area fraction were carried out using the Image-Pro-Plus analysis software.[24]

For SEM observations and EBSD measurements, the specimens were first mechanically polished and then electro-polished with a solution of 20% perchloric acid in methanol for 6 s under a voltage of 35 V at 10 °C. Measurements were performed on a JSM-6500F-SEM with an OXFORD EBSD acquisition camera and the OXFORD-AZTEC acquisition software. To study the effect of deformation on the composition

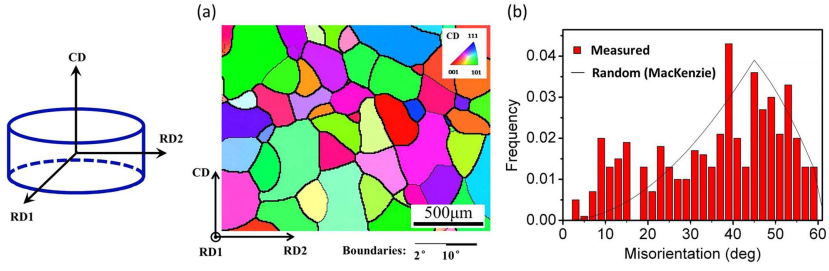

Fig. 1. (a) EBSD map of the single β phased microstructure of Ti–5553 after solution treatment. (b) Corresponding histogram of correlated misorientation angle distribution.

distribution and the formation mechanism of the precipitate free zones (PFZs), the distributions of the alloying elements were examined by EDX, using a Zeiss Supra-40 SEM equipped with a Bruker-QUANTAX SDD-EDX detector and the software Esprit (Bruker), v 1.9.4. In order to remove the residual stress induced by the mechanical polishing, further polishing with oxide polishing suspension (OPS) was conducted on an automatic polishing machine (Struers Tegramin-25) at a rotation speed of 200–300 rpm for 20 min. The polished specimens were rinsed with tap water for 10 min and then cleaned in ethanol in an ultrasonic bath for 30 min. Chemical composition mappings were carried out in the areas of 47 × 100 μm, with one a step size of one micrometer. At each measuring point, a 35 000 counts X-ray spectrum is recorded. For each chemical element, compositions were estimated from peaks intensities, comparing with 1 000 000 counts pure standards spectra, according to a classical PhiRhoZ method.[25] For precise phase analyses, 1 000 000 counts punctual spectra were recorded. Writing N as the number of counts of a X-ray peak of one chemical element, relative precision for composition c is about then $\frac{\Delta c}{c} = \left(\frac{1}{\sqrt{N}}\right)_{sample}$.

TEM thin foils were prepared first by mechanical thinning to about 100 μm in thickness. Then discs with 3 mm in diameter

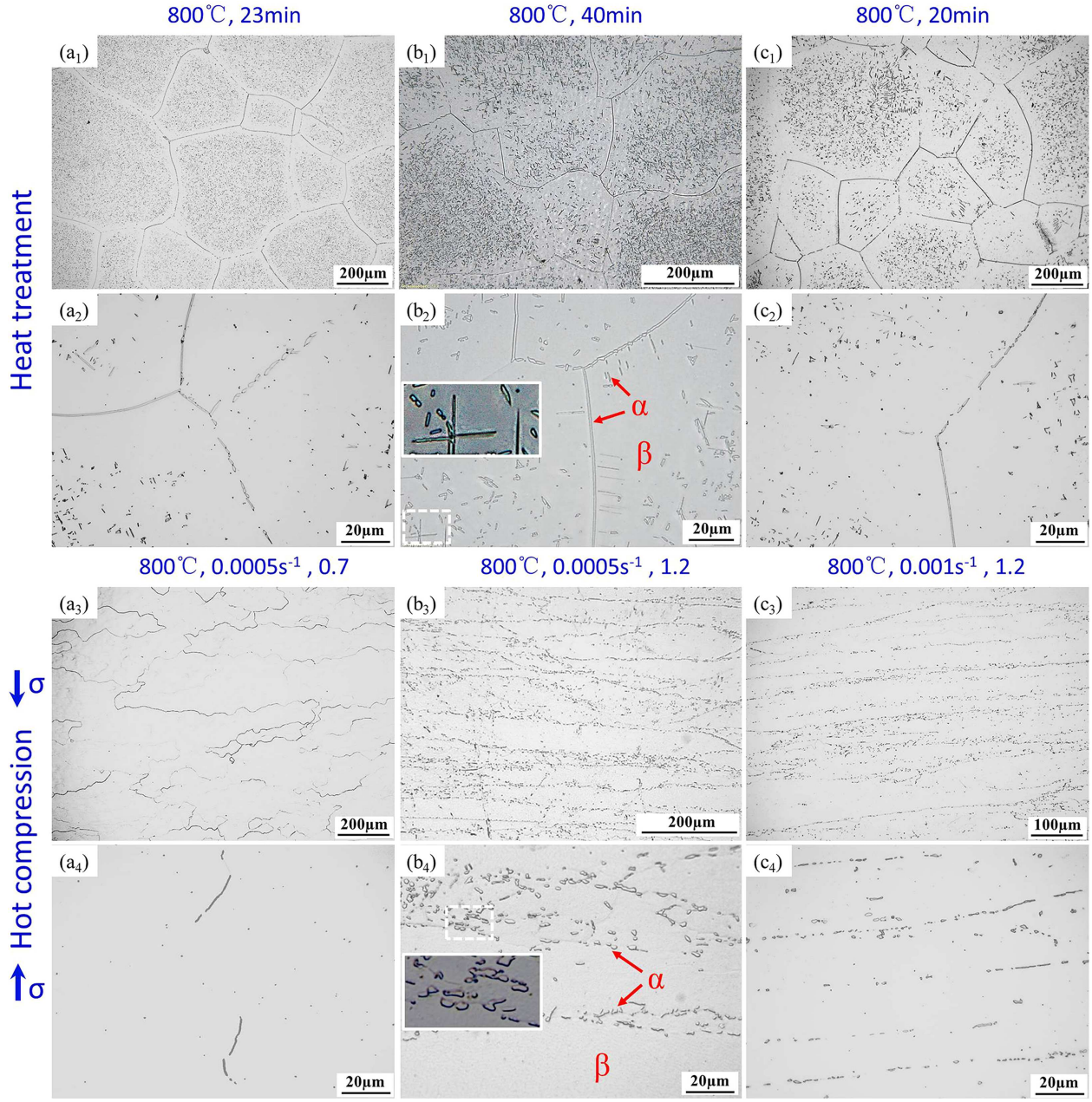

Fig. 2. Optical microstructure: heat treatment at 800 °C microstructure with 23 min (a_1–a_2), 40 min (b_1–b_2), and 20 min (c_1–c_2), and their corresponding hot compression microstructure at 800 °C with 0.0005 s^{-1}, 0.7 (a_3–a_4), 0.0005 s^{-1}, 1.2 (b_3–b_4), and 0.001 s^{-1}, 1.2 (c_3–c_4). The inserted figures are the magnifications of the region marked with white rectangle.

were punched off and further thinned to be electron trans parent by twin-jet electro-polishing using a Struers Tenupol-5 twin-jet electropolisher in a solution of 20% perchloric acid in methanol under 10 V at −35 °C. TEM observations were performed on a Philips CM200 TEM operated at 200 kV.

3. Results

3.1. Initial Microstructure of Ti–5553

To obtain the single β initial microstructure, prior to any thermo-mechanical treatment, a solution treatment at 900 °C for 30 min followed by water quenching was performed. The resulting microstructure displayed in Figure 1a is composed of single β equiaxed grains with an average size of ≈300 μm. The sampled grains did not allow to measure the texture precisely, but the correlated misorientation angle distribution histogram in Figure 1b is close to that of randomly oriented polycrystals (the line profile), suggesting that the alloy is probably not sharply textured.

3.2. Morphology and Distribution of α

Each column of Figure 2 represents the optical micrographs of the microstructures obtained for the same holding time at 800 °C either through heat treatments (Figure 2a_1–c_2) or hot compressions (Figure 2a_3–c_4). Each microstructure is represented at two different magnifications. It is seen that for the heat treated samples, the α phase forms mainly along β grain boundaries and also inside the β grains. The grain boundary α (α_{GB}) are near continuous along the grain boundaries, whereas the intragranular α (α_I) precipitates have a short plate or particle shape (Figure 2b_2). With increasing aging time (from 20 to 40 min), the amount of both kinds of α precipitates increases. The α_{GB} precipitates become more continuous, and the α_I increase both in size and number (Figure 2a_2–c_2). Moreover, with the prolongation of the aging time, some parallel α lamellae start to precipitate from grain boundary toward grain interior, forming the so-called Widmanstätten α, α_{WGB} (Figure 2b_2). All these characters are typical characteristics of the β → α transformation in Ti–5553 alloy and of some other Ti alloys. Additionally, one can find that in all the heat treated samples, PFZs are present on either side of β grain boundaries with a thickness of about 40 μm (Figure 2a_1–c_2), suggesting that the formation of α precipitates is diffusional.

When the isothermal compression is applied, the resultant microstructures change drastically compared with heat treated microstructures. The chosen reference treatment was performed with a strain of 1.2 and a strain rate of 0.0005 s^{-1} and is in the central column of Figure 2b_3 and b_4. Comparison at iso-strain and iso-strain rate can be made with the micrographs presented in Figure 2a_3, a_4 and c_3, c_4, respectively.

All deformed states have several characteristic in common. The β grains became elongated in the direction perpendicular to the compression axis, and its boundaries are no longer straight. The aspect ratio of the grains increases with increasing strain, as shown in the SEM backscattered electron (BSE) micrographs (Figure 3). In this figure, the contrast is mostly due to the difference in crystallographic orientation and, thus, can be utilized to identify grains and subgrains. These indicated that DRV/DRX happened with the deformation by comparing the Figure 1–3.[6,8,9] At small deformation strain (0.7), the elongation of the β grains is accompanied by grain fragmentation, forming subgrains (Figure 3a) which is typical of DRV. With the strain increasing to 1.2, banded structures with their longer axis perpendicular to the compression axis formed. Within each band, sub domains with different sizes and shape can be clearly seen (Figure 3b). The width of the bands is around 40 μm, which is of the same order of magnitude as the PFZs on either side of the β grain boundaries in the heat treated specimens.

Together with the morphology change of the β grains, the β → α phase transformation occurred dynamically. First, unlike in the undeformed specimens, a large majority of the precipitates are located along β boundaries (both HAGBs and LAGBs), but seldom in β grain interiors (Figure 2a_3,a_4–c_3, c_4). The morphology of the precipitates differs from those in the corresponding heat treated specimens. Almost α phase are equiaxed or short rod shaped and 1–2 μm in length (Figure 3d). As the TEM micrograph shows that, moreover, no other finer α precipitates nucleated in the β matrix. Such a microstructure is often referred as "necklace" microstructure.[26] With increasing

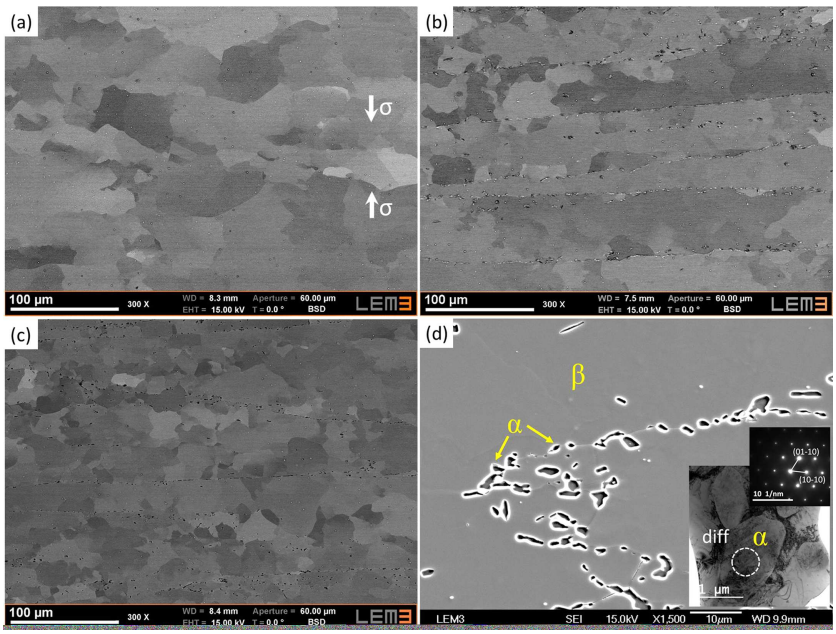

Fig. 3. SEM back scattered electron (BSE) micrographs of Ti–5553 samples hot compressed at 800 °C to a strain of (a) 0.7 under a strain rate of 0.0005 s^{-1}, (b) 1.2 under a strain rate of 0.0005 s^{-1}, (c) 1.2 under a strain rate of 0.001 s^{-1}, (d) secondary electron (SE) micrograph of "necklace" microstructure at 0.0005 s^{-1} deformed to 1.2. TEM bright field micrograph and SAED pattern of α phase are insetted.

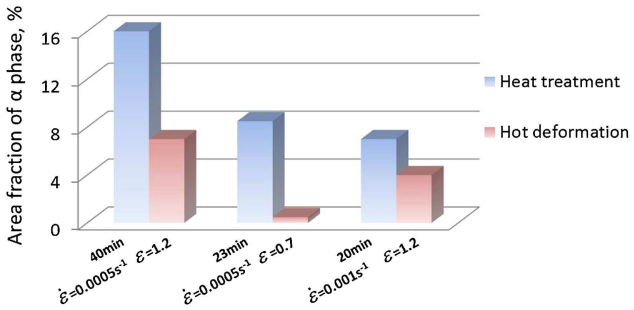

Fig. 4. Area fractions of α phase in hot deformed and the corresponding heat treated specimens.

strain, the isothermal holding time also increases. As consequence, the α precipitates are more numerous but remains discontinuous.

The strain rate has only a moderate influence on the microstructures. A comparison has been made between the microstructures obtained at a strain of 1.2, with a strain rate changing from 0.0005 to 0.001 s^{-1}. At higher strain rate, there are less α particles (≈1 μm) and they are smaller. This is related to the shorter isothermal holding time and, thus, a shorter available time for the formation and the growth of the α phase. For the β matrix, as seen in Figure 3c, grains are largely refined as the case under slow deformation rate (Figure 3b), indicating that DRV/DRX occurred with the deformation. However, the banded structure (Figure 3c) is less visible on the optical micrographs than that of lower strain rate (Figure 3b). This is because the lower fraction of α phase, hence its decoration effect on microstructure and its pinning effect on β grain boundaries is reduced.

3.3. $\beta \rightarrow \alpha$ Transformation Amount

The influence of the deformation on the phase transformation process is further studied. The amount of α precipitates are quantified in the hot compressed samples and in their heat treated counterparts. The results are shown in Figure 4. It is seen that, in general, the amount of α precipitates in the deformed samples is less than that obtained under heat treatment, indicating that the deformation at 800 °C could retard the $\beta \rightarrow \alpha$ phase transformation. The area fractions of the α phase in the specimens heat treated at 800 °C for 23 min and that hot compressed under the same thermal conditions but with a strain of 0.7 under the strain rate of 0.0005 s^{-1} are ≈8.5 and ≈0.5%, respectively. When the strain was increased to 1.2 (40 min), the corresponding area fractions of the heat treated and the hot compressed specimens are ≈16 and ≈7%. When the deformation rate increases to 0.001 s^{-1}, the areas fraction of the α phase in the hot compressed specimen and that in the corresponding heat treated specimen are ≈4 and ≈7%, respectively. Comparing the range of the drops, one can find that the drop is obviously smaller, when strain rate is 0.001 s^{-1}. This indicates that retardation impact of deformation on phase transformation with higher strain rate is lower.

To investigate the effect of strain on the phase transformation amount further, the variation of α morphologies along the compression disc radius and thickness are shown in Figure 5. It can be seen that the α particles precipitate in the whole specimen. However, the α phase area fractions in different zones are obviously different. It is well known that zone *b* has the larger strain than *a* and *c* because *b* is closer to the center of the deformation specimen. Actually, the amount of α phase in zone *b* is least (Figure 5b). That fully indicated that deformation inhibited $\beta \rightarrow \alpha$ phase transformation at 800 °C significantly.

3.4. Chemical Composition Distribution Characteristics

To study the effect of deformation on the composition distribution and the formation mechanism of the PFZs, the distribution and evolution of alloying elements (Ti, Al, Mo, V, Cr, and Fe) by SEM/EDX analyses are shown in Figure 6. Obviously, the α and β stabilizing elements, Al and Mo, are enriched and depleted in the α phase, respectively, (Figure 6a,d).[27] It happens both in heat treated and hot compressed specimens, confirming that the phase transformation was diffusional and deformation did not change it.

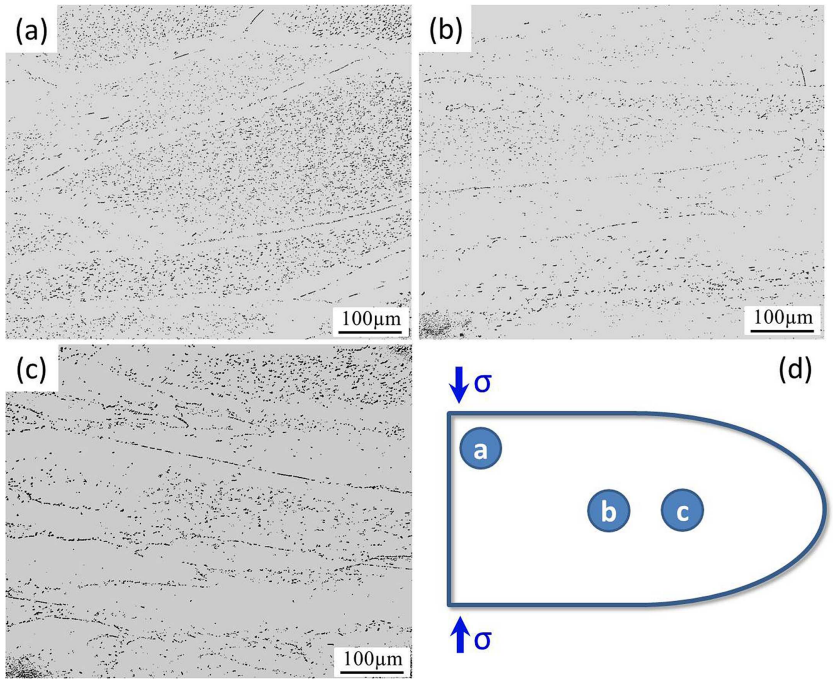

Fig. 5. Variation of α morphologies along the compression disc radius and thickness: (a) area a along the thickness near the edge of the specimen; (b) area b along the radius near the central of the specimen; (c) area c along the radius near the edge of the specimen; (d) the schematic of observation surface.

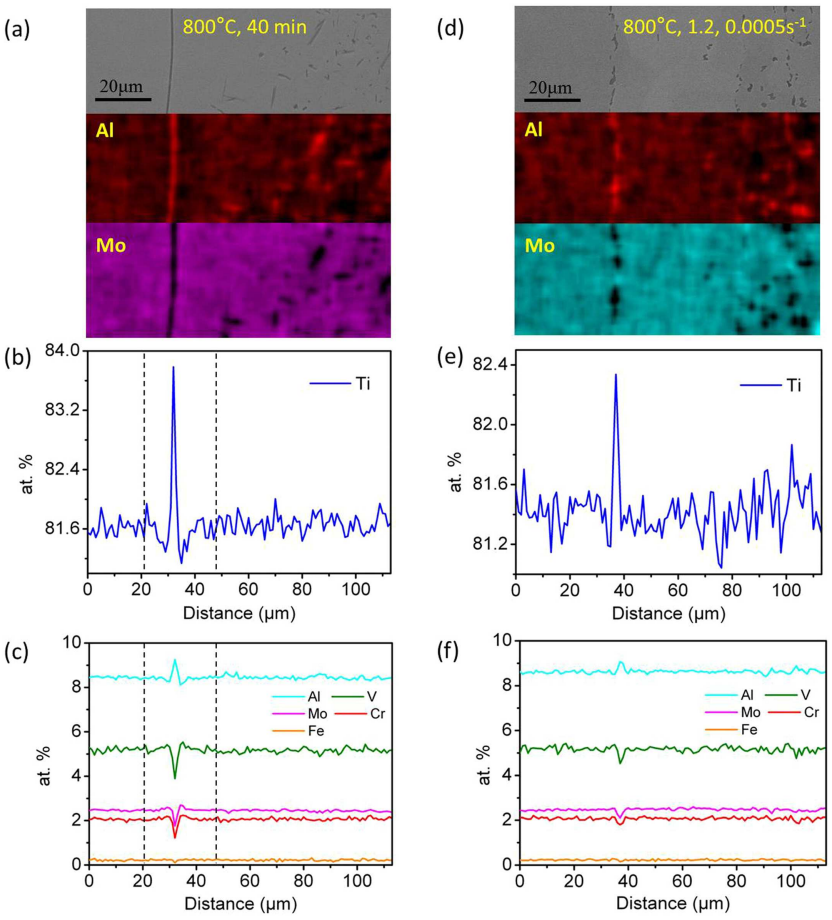

Fig. 6. SEM/EDX Al and Mo composition maps (a) heated treated at 800 °C for 40 min and (d) hot compressed at 800 °C to a strain of 1.2 at a strain rate of 0.0005 s^{-1} and the corresponding line profiles of Ti, and the alloying elements Al, Mo, V, Cr, and Fe in (b) and (c) the heat treated, and (e) and (f) the hot compressed specimens integrated along the direction parallel to the boundary (vertical in (a) and (d)).

For the heat treated specimen, Ti and Al are depleted in the zones ≈10 μm in width adjacent to the β boundaries, as indicated with the dotted lines in line profiles Figure 6b and c. In contrast, the β stabilizing elements (Mo, V, Cr, and Fe) are enriched in these areas. These distribution features lead to the formation of PFZs on both sites of β grain boundaries. For the hot compressed specimen, quantitative analysis of the α precipitates shown in Table 1 demonstrates that the enrichment of the α stabilizing element and the depletion of the β phase stabilizing elements in the α phase is more pronounced. This may be attributed to the existence of large amount of crystal defects produced by deformation. The abundant defects, such as dislocations and subgrain boundaries, could provide favorable diffusion paths and enhance the segregation of the alloying elements required by phase transformation.

3.5. Orientation Relationship between α/β and Their Crystallographic Features

Crystallographic analyses show that for the heat treated specimens, the α phase and the β phase respect the BOR. As shown in Figure 7a and b, both the α_I and the α_{GB} demonstrate good agreement with the BOR. The deviations are smaller than 4°. The peak at 13° comes from the α_{GB}, which respect strictly the BOR only with one β grain. However, the relation with the other grain is not completely random. Indeed, in special geometric cases, a α_{GB} can respect the BOR with both β grains. In cases where the geometrical conditions are approximately met, there is a tendency to minimize the BOR with respect the second β grain also.[28]

When hot compression is performed, the performance totally changes. As shown in Figure 7c and d, most of the α particles are deviated from the BOR. About 66% of the α phase have a deviation larger than 10° (regarded as a large deviation form BOR) and the maximum deviation reaches 42° (Figure 7d). From the EBSD band, contrast images of the microstructures obtained by the heat treatment and the hot compression in Figure 7a and c, the width of the PFZs is in comparable dimension as the width of bands in the latter.

Examinations also show that the deviation from the BOR is strain and strain rate dependent. As shown in Table 2, with the increase of the deformation strain from 0.7 to 1.2 under a constant strain rate 0.0005 s^{-1}, the amount of α having a deviation higher than 10° are increased from 26 to 66%. At

Table 1. Chemical composition of α phase in heat treatment and hot compressed specimens (at%)

		Heat treated		Hot compressed
Alloy elements	Nominal composition	α_{GB}	α_I	α_{GB}
Titanium	80.94	82.75 ± 0.4	83.46 ± 0.4	86.92 ± 0.4
Chromium	2.52	1.42 ± 0.2	1.33 ± 0.2	0.13 ± 0.2
Molybdenum	2.46	2.13 ± 0.1	1.70 ± 0.1	0.30 ± 0.1
Iron	0.36	0.11 ± 0.02	0.01 ± 0.02	0 ± 0.02
Vanadium	4.46	3.89 ± 0.2	3.73 ± 0.2	1.65 ± 0.2
Aluminum	9.26	9.70 ± 0.3	9.78 ± 0.3	11.00 ± 0.3

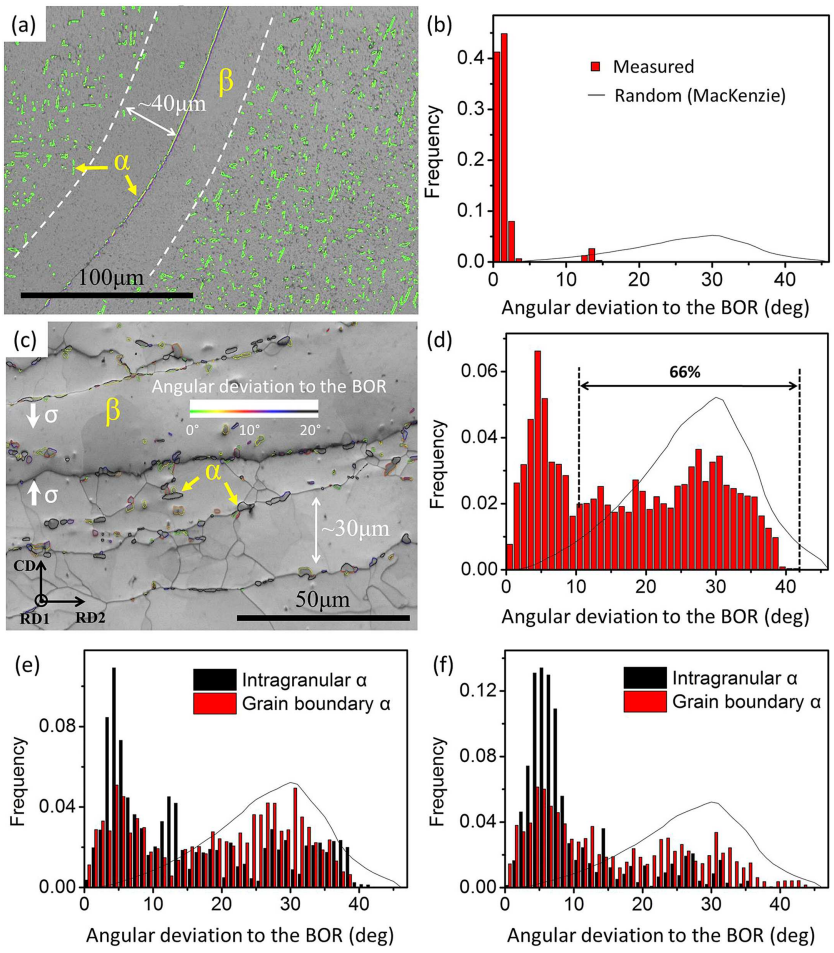

Fig. 7. EBSD Band contrast micrograph of Ti–5553 (a) heat treated at 800 °C for 40 min and (c) hot compressed at 800 °C to a strain of 1.2 under a strain rate of 0.0005 s^{-1}, and (b) and (d) the corresponding histograms of angular deviation from the BOR between α and β in the two specimens. The colored contour lines around α indicate the angular deviations with respect to the exact BOR. The white dashed lines in (a) delimitate the PFZs on both sides of the boundary β. (e) (f) Statistical histogram of the angular deviation of

constant strain, when the strain rate increases from 0.0005 to 0.001 s^{-1}, the amount of α grains deviated with more than 10° from the BOR decreases from 66 to 51%.

Two distinct mechanisms may accommodate the macroscopic strain at high temperature. One is dislocation slip and the other is grain boundary sliding. The latter contribution increases with decreasing of the strain rate and, hence, more boundary α losses their OR with the adjacent β grains. As the α phase is known to respect the BOR when it precipitates, it indicates that the OR is gradually destroyed during the subsequent deformation due to grain boundary sliding and dislocation ship in the area around the α particles. This has been further confirmed by the subsequent examinations, where the deviations of the α_I and the α_{GB} are analyzed separately. The results shown in Figure 7e and f clearly demonstrate that the deviation mainly happens to α_{GB} phase and the amount of α with large deviation (>10°) decreases with the increase of the deformation strain rate. Moreover, there are two other reasons that explain the difference α_I and the α_{GB}. The first one is that precipitation occurs first at grain boundaries. Then, the first precipitates have more time to undergo the subsequent deformation; the second one is that there is already one side of the GB which is not in BOR with the precipitate as it formed.

During the deformation, the morphology and the crystallographic orientation of the α_{GB} also changed from a continuous layer with single orientation (Figure 8a) to particles having each a different crystallographic orientation Figure 8b. For example, those in the white dotted box in Figure 8b, these α grains are in different colors in the magnifying IPF map and have own different $\{0001\}_\alpha$ plane shown in the $\{0001\}_\alpha$ pole figure. Furthermore, the adjacent α particles along the β grain boundary are neither in BOR nor twin related, for instance 63.6°/[341] and 38°/$[\bar{1}\bar{4}0]$ in axis/angle pairs. Thus, hot deformation not only changed the nucleation site of α phase, but also destroyed the OR.

TEM examinations revealed that the β matrix possesses deformed and DRV/DRX substructures. As shown in Figure 8c, many β grains are composed of bands characterized by large amount of parallel dislocation arrays, demonstrating the mixed feature of deformation, and polygonalization. The large quantities of dislocations were induced by deformation; whereas their regular arrangement should results from polygonalization. In some other areas, DRV/DRX is in progress. Equiaxed grains of several micrometers in size are formed, as shown in Figure 8d, indicating the occurrence of DRV/DRX. Thus, dynamic hardening and dynamic softening occurred simultaneously. As aforementioned in Section 3.2, due to the increased atomic mobility at high temperature, softening processes, such as DRV and DRX would occur during high temperature deformation. That agrees with that it is generally accepted that the predominating softening mechanism of the β phase is DRV in metastable β titanium alloys.[3] Moreover, the DRX could be identified as typical continuous dynamic recrystallization

Table 2. Deviation from BOR under different deformation parameters

	Variations of deformation parameters			
	Strain rate of 0.0005 s^{-1}		Strain of 1.2	
Deviation from BOR	0.7	1.2	0.001 s^{-1}	0.0005 s^{-1}
Fraction >10(%)	26	66	51	66

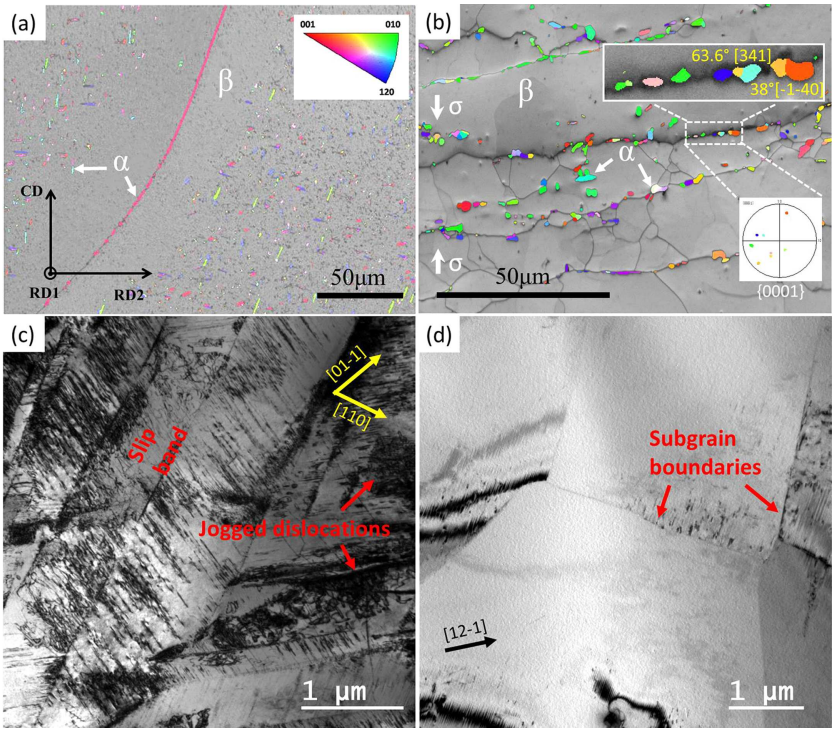

Fig. 8. EBSD micrographs of Ti–5553 (a) heat treated at 800 °C for 40 min, (b) hot compressed at 800 °C to a strain of 1.2 under a strain rate of 0.0005 s^{-1}. In the figures, the β phase is represented by the EBSD band contrast and the α phase is by the Y_0 axis inverse pole figure (IPF) micrograph. (c) (d) TEM bright field micrographs of Ti–5553 hot compressed to 0.7 under the strain rate of 0.0005 s^{-1}.

(CDRX), which involves a transformation of low angle boundaries into high angle boundaries of the subgrains.[9,29] Due to this instability during continuous deformation, the nucleated α cannot grow smoothly to form continuous precipitates. Moreover, the abundant dislocations produced by the deformation offer efficient diffusion paths allowing quick segregation of the alloying elements to the boundary areas, as indirectly confirmed by the results in Table 1.

4. Discussions

4.1. Influence of Deformation on Morphology and Nucleation Site of α Precipitates

Generally speaking, the nuclei would be double-spherical cap shape on the GBs when α/β has an incoherent interface (Figure 9a), which could decrease the interfacial energy. The α/β interface maintains the BOR with the α_{GB} maintain the flat plane and the another β grain has the incoherent interface with α precipitates show a spherical cap shape (Figure 9b). In special cases, the α_{GB} could maintain the BOR with both β grains,[30] which should be the most energetically preferred configuration. As the present result shown above, the majority of α phase have a large deviation from exact BOR, which vitally result in the equiaxed or rod shaped α at the GBs. The α precipitates on GBs during thermo-mechanical processing are inclined to grow as particles instead of plates for decreasing the interfacial energy due to their non-coherent phase boundaries. In heat treated Ti–5553 alloy, instead, intragranular α precipitates develop into plate shape during growth due to their orientation relationship with the β matrix, coherency state, and the associated anisotropy in the interfacial energy, elastic strain energy, and growth kinetics. Lengthening of the plates occurs by the addition of atoms at the incoherent risers of ledges at the tips of the plates and thickening results from the movement of growth ledges across the broad semi-coherent interfaces.[28,31,32]

As seen in Figure 3 and 8, the initial coarse β grains are filled with large amount of LAGBs and HAGBs, and the β boundaries are serrated with large amount of boundary ledges and steps. On one hand they offer favorable individual nucleation sites, but on the other hand they prevent the already formed α particles to grow smoothly to reach their neighboring particles and to form continuous α along the boundary.

Moreover, the long rod shaped α_{GB} might be fragmented and spherized to globular particles during deformation, which was associated primarily with the classical boundary splitting mechanism followed by further spheroidization of a particles by means of termination migration.[33–36] The kinetics of α plates fragmentation during deformation also depends upon the nature of the α/β interphase boundaries.[21] Loss of coherency of the α/β interphase boundaries with increasing stress intensifies dynamic fragmentation of the lamellar microstructure due to (i) the hindering of dislocation movement across non-coherent α/β interfaces

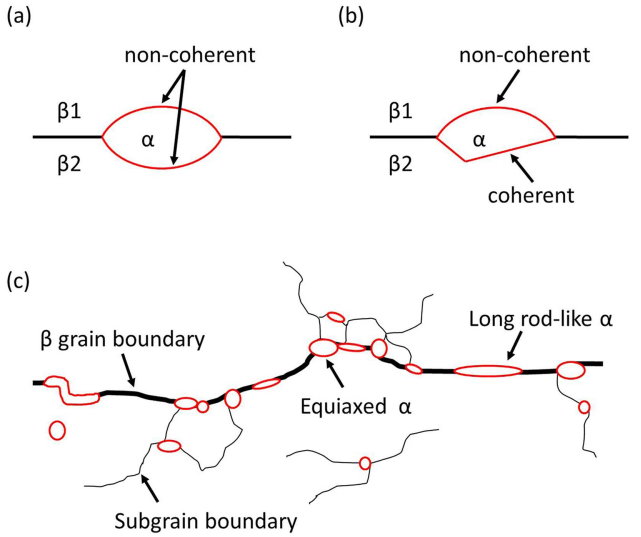

Fig. 9. Schematic diagram: (a) (b) α phase precipitates on β grain boundaries, (c) "necklace" microstructure.

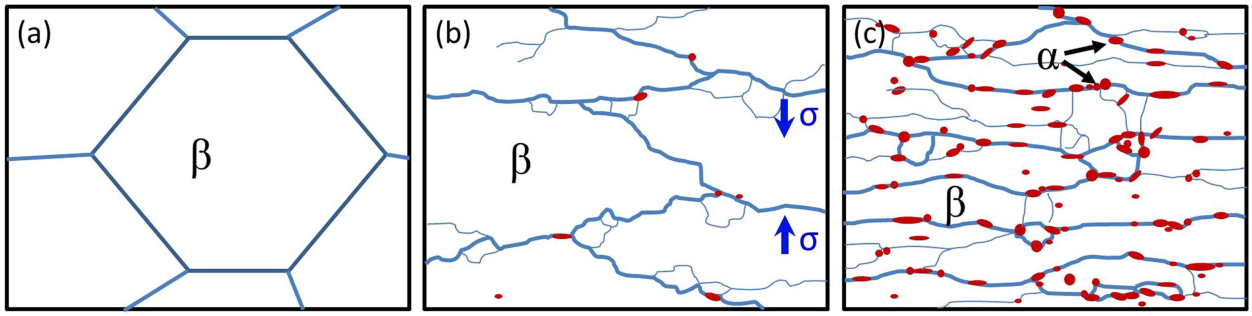

Fig. 10. Illustration of the microstructural evolution of Ti–5553 alloy during the hot compression at 800 °C. (a) Initial microstructure composed of single β equiaxed grains, (b) β grain fragmentation through deformation and DRV/DRX and commencement of α precipitation at β boundaries, and (c) formation of band shaped β grains with particle shaped α (in red) along β boundaries.

and (ii) a concomitant increase in the interphase boundary energy. According the above contributions, thus, the formed α along the β boundaries would be discontinuous and in particle shape.

Another big difference is the nucleation sites of α phase between undeformed and thermo-mechanical processing specimens. This difference is contributed complexly to two main aspects: (i) Almost all the spacing between the boundary segments in deformed microstructure are lower than 40 μm, that is roughly the thickness of the PFZ (Figure 7). Meanwhile, large amount of crystal defects, especially dislocations are produced, offering efficient diffusion channels (Figure 8). In this sense, the segregation of alloying elements are more efficient (Table 1), hence α phase forms mainly at LAGBs and HAGBs and very rarely in grain interiors. (ii) Deformation would be stopped before the nose of the *c*-curve (TTT curve), which indicates that α precipitation within the β matrix is not crossed.[26] Thus, after deformation, discontinuous α particles is only present at the β grain boundaries, but not within the β grains. Due to the specific influences of deformation on α nucleation sites and α morphology, the characterized "necklace" microstructure is obtained, as illustrated in Figure 9c.

4.2. Influence of Deformation on Orientation Relationship between α and β

The results of the present study suggests that at the beginning of the formation of α, the BOR is maintained as the case of in the heat treated specimens, however, with the deformation, the BOR is gradually lost. The deformation was mainly accommodated by the β phase due to the relatively smaller size and less volume fraction of α phase. As the present deformation temperature is relatively high (800 °C, i.e., higher than the recrystallization temperature of this alloy). The high deformation temperature gives rise to the occurrence of DRV that reorganization of dislocations leading to rotation of the crystalline lattices. Moreover, the stress concentration on grain boundaries are more heavy than the grain interiors, the different mechanical properties of β and α lead to the uncoordinated migration of the β/β segments and the β/α segments.[20] In this way, the BOR between β/α was destroyed gradually (Figure 6,7 and Table 2).

4.3. Deformation Induced Phase Transformation Retardation

The above results show that during the hot compression of the present Ti–5553, the β phase was subjected to three processes: deformation, dynamic softening (DRV and DRX), and β → α phase transformation. The phase transformation is obviously retarded (Figure 4), which is contrary to the understanding of deformation induced phase transformation.[10] From the Section 3.2, we did not find that the β → α phase transformation happened immediately with the starting of the deformation (Figure 2a$_3$). Whereas, DRV/DRX of the β phase under deformation happened significantly. That is, to say that DRV/DRX happened before the β to α phase transformation at 800 °C deformation. The phase transformation just started when DRV/DRX is well advanced. This indicates that the energy barrier of DRV/DRX is smaller than that to phase transformation. Another strong evidence is that the reduced retardation effect of the deformation on phase transformation under higher strain rate corresponds to the reduced degree of DRV/DRX of the β phase. It seems that the β → α phase transformation is in competition with the DRV/DRX of the β phase under 800 °C deformation. For convenience, the microstructural evolution induced by deformation, DRV/DRX and phase transformation of the

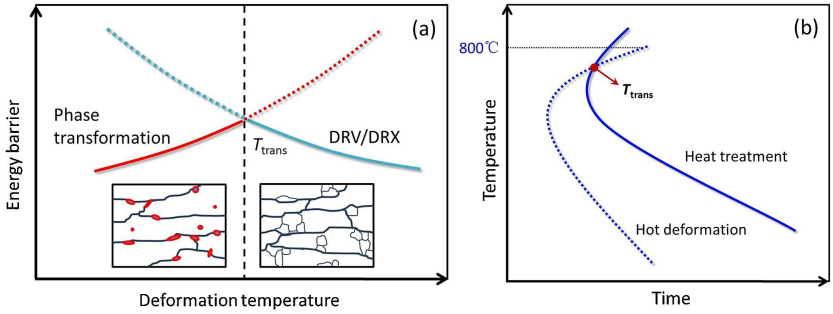

Fig. 11. (a) Illustration of the completion between DRV/DRX and phase transformation; (b) TTT schematic diagram under the heat treatment and thermo-mechanical conditions.

present alloy during hot deformation at 800 °C is summarized in Figure 10.

Thermodynamically, Gibbs free energy change ΔG of a transformation under deformation can be expressed as $\Delta G = V\Delta G_V + A\Delta G_r + V\Delta G_s + \Delta G_d$, where ΔG_V, ΔG_r, and ΔG_S are the volumic free energy change, interfacial energy, and elastic strain energy, respectively, and ΔG_d is the stored energy provided by deformation. ΔG_V and ΔG_d represent the driving force for the transformation, whereas ΔG_r and ΔG_S the energy barriers to the transformation. Under the present deformation (at 800 °C), although the driving force for phase transformation is increased by the addition of the stored energy provided by deformation, the DSIPT did not happen, but on the contrary it was retarded. This is due to the occurrence of DRV/DRX induced by hot deformation. Actually, the two transformation processes, DRV/DRX and $\beta \rightarrow \alpha$ transformation, occurred competitively during the hot compression. Although the two processes are diffusive in nature, the efforts required to achieve the two are not the same. For softening, it is a restoration process, reducing the quantity of defects in crystals. It involves neither segregation of alloying elements nor collective crystal structure change, as the case of β to α phase transformation. The energy barrier for DRV/DRX is smaller. Therefore, it requires lower driving force to overcome the energy barriers. The stored energy provided by the deformation is firstly consumed by softening, before it reaches the level, that is, sufficient to drive the phase transformation.[6,37] In this way, the phase transformation is retarded. It should be noted that the two transformations have inverse temperature dependence. For DRV/DRX, it occurs above the theoretical temperature and the driving force increases with the increase of the actual temperature, whereas for β to α phase transformation, the effective transformation temperature is lower than the equilibrium temperature and the driving force increases with the decrease of the temperature. Thus, there should be a transition temperature (T_{trans}) above which DRV/DRX is prevalent and phase transformation inhibited, but below which DRV/DRX is suppressed and phase transformation promoted, as illustrated by Figure 11a.

Fundamentally, the kinetics of $\beta \rightarrow \alpha$ phase transformation is changed by the application of deformation. As the TTT schematic diagram Figure 11b shows, above the T_{trans} (800 °C), DRV/DRX is prevalent and phase transformation inhibited. Whereas, below the T_{trans}, DRV/DRX is suppressed and phase transformation enhanced. That is why the DSIPT occurs as observed in some hot deformation process of Ti alloys.[10]

Clearly other deformation parameters, such as strain and strain rate, may have also influence on the T_{trans}, depending on their kinetic effect on the softening process. Large strain and high strain rate would inhibit the softening process, thus, reduces the retarding effect of phase transformation.

5. Conclusions

The $\beta \rightarrow \alpha$ phase transformation of metastable β titanium alloy Ti–5553 during thermo-mechanical treatments at 800 °C, in terms of nucleation site, morphology, orientation relationship, and transformation kinetics was studied. The following conclusions can be drawn:

1) During the deformation at 800 °C temperature in the $\alpha + \beta$ region, equiaxed or short rod shaped α precipitates (1–2 μm) on the high and low angle grain boundariesm, but seldom in β grain interiors, forming a "necklace" microstructure. This is due to the increase of low angle and high angle boundaries produced by deformation and subsequent DRV/DRX. This provides also abundant nucleation sites. The defects induced by the hot compression also provide favorable diffusion paths for the segregation of the alloying elements and accelerate the segregation of the elements to the boundaries. As the deformation and the subsequent DRV/DRX happen in a continuous manner, boundary migration take place continuously. Then, the nucleated α cannot grow smoothly to form continuous precipitates.
2) The deformation and the subsequent DRV/DRX which happen in a continuous manner, destroys the BOR gradually between the α and β phases. The deviation of α_{GB} is larger than that of α_I. This is due to the continuous deformation and recrystallization that induces β grain migration and rotation. The coherency of the α/β interfaces is reduced due to the different and uncoordinated lattice rotation at β/β and β/α boundaries. The deviation from the BOR increases both with increasing strain and decreasing strain rate.
3) The phase transformation is obviously retarded during the hot compression due to the competitive effect of softening process. The kinetics of $\beta \rightarrow \alpha$ phase transformation is changed by the application of deformation. Due to the inverse temperature dependence of the two transformations, there could exist a transition temperature (T_{trans}), above which the driving force for phase transformation is smaller than that for DRV/DRX, whereas below which the DRV/DRX is retarded. This competition mechanism is not only found for the deformation temperature but also strain and strain rate, which is not only applicable in the present Ti–5553 alloy, but also other hot deformed Ti alloys.

Article first published online: xxxx
Manuscript Revised: February 9, 2017
Manuscript Received: December 22, 2016

[1] T. Gloriant, G. Texier, F. Prima, D. Laillé, D. M. Gordin, I. Thibon, D. Ansel, *Adv. Eng. Mater.* **2006**, *8*, 961.
[2] J. D. Cotton, R. D. Briggs, R. R. Boyer, S. Tamirisakandala, P. Russo, N. Shchetnikov, J. C. Fanning, *JOM* **2015**, *67*, 1281.

[3] M. Jackson, R. Dashwood, L. Christodoulou, H. M. Flower, *Metall. Mater. Trans. A* **2005**, *36*, 1317.
[4] M. Salib, J. Teixeira, L. Germain, E. Lamielle, N. Gey, E. Aeby-Gautier, *Acta Mater.* **2013**, *61*, 3758.
[5] Z. Huda, P. Edi, *Mater. Des*. **2013**, *46*, 552.
[6] N. G. Jones, R. J. Dashwood, D. Dye, *Mater. Sci. Eng. A* **2008**, *490*, 369.
[7] J. Coakley, V. A. Vorontsov, K. C. Littrell, R. K. Heenan, M. Ohnuma, N. G. Jones, D. Dye, *J. Alloys Compd*. **2015**, *623*, 146.
[8] C. Poletti, L Germain, F. Warchomicka, M. Dikovits, S. Mitsche, *Mater. Sci. Eng. A* **2016**, *651*, 280.
[9] J. K. Fan, H. C. Kou, M. J. Lai, B. Tang, H. Chang, J. S. Li, *Mater. Sci. Eng. A* **2013**, *84*, 121.
[10] A. Dehghan-Manshadi, R. J. Dippenaar, *Mater. Sci. Eng. A* **2012**, *552*, 451.
[11] O. M. Ivasishin, P. E. Markovsky, Y. V. Matviychuk, S. L. Semiantin, *Metall. Mater. Trans. A* **2003**, *34*, 147.
[12] H. S. Zurob, Y. Brechet, G. Purdy, *Acta Mater.* **2001**, *49*, 4183.
[13] W. Chen, Q. Sun, L. Xiao, J. Sun, *Mater. Sci. Eng. A* **2010**, *527*, 7225.
[14] W. G. Burgers, *Physica* **1934**, *1*, 561.
[15] T. Furuhara, T. Ogawa, T. Maki, *Philos. Mag. Lett*. **1995**, *72*, 175.
[16] M. R. Daymond, R. A. Holt, S. Cai, P. Mosbrucker, S. C. Vogel, *Acta Mater.* **2010**, *58*, 4053.
[17] I. Lonardelli, N. Gey, H. R. Wenk, M. Humbert, S. C. Vogel, L. Lutterotti, *Acta Mater.* **2007**, *55*, 5718.
[18] N. Stanford, P. S. Bate, *Acta Mater.* **2004**, *52*, 5215.
[19] S. Suri, G. B. Viswanathan, T. Neeraj, D. H. Hou, M. J. Mills, *Acta Mater.* **1999**, *47*, 1019.
[20] S. Zherebtsov, G. Salishchev, S. L. Semiatin, *Philos. Mag. Lett*. **2010**, *90*, 903.
[21] M. Cabibbo, S. Zherebtsov, S. Mironov, G. A. Salishchev, *J. Mater. Sci*. **2013**, *48*, 1100.
[22] D. He, J. C. Zhu, S. Zaefferer, D. Raabe, Y. Liu, Z. L. Lai, X. W. Yang, *Mater. Sci. Eng. A* **2012**, *549*, 20.
[23] M. Klimova, S. Zherebtsov, G. Salishchev, S. L. Semiatin, *Mater. Sci. Eng. A* **2015**, *645*, 292.
[24] http://www.mediacy.com.cn/cn/index/index.asp.
[25] J. L. Pouchou, F. Pichoir, in *Electron Probe Quantitation*, Springer, US **1991**, p. 31.
[26] C. Sauer, G. Luetjering, *J. Mater. Process. Technol*. **2001**, *117*, 311.
[27] A. Carman, L. C. Zhang, O. M. Ivasishin, D. G. Savvakin, M. V. Matviychuk, E. V. Pereloma, *Mater. Sci. Eng. A* **2011**, *528*, 1686.
[28] R. Shi, V. Dixit, G. B. Viswanathan, H. L. Fraser, Y. Wang, *Acta Mater.* **2016**, *102*, 197.
[29] S. Gourdet, F. Montheillet, *Acta Mater.* **2003**, *51*, 2685.
[30] D. Bhattacharyya, G. B. Viswanathan, H. L. Fraser, *Acta Mater.* **2007**, *55*, 6765.
[31] T. Furuhara, S. Takagi, H. Watanabe, T. Maki, *Metall. Mater. Trans. A* **1996**, *27*, 1635.
[32] G. Spanos, R. Masumura, R. Vandermeer, M. Enomoto, *Acta Metall. Mater.* **1994**, *42*, 4165.
[33] S. Zherebtsov, M. Murzinova, G. Salishchev, S. L. Semiatin, *Acta Mater.* **2011**, *59*, 4138.
[34] S. Roy, S. Suwas, *J. Alloy Compd*. **2013**, *548*, 110.
[35] J. K. Fan, H. C. Kou, M. J. Lai, B. Tang, H. Chang, J. S. Li, *Mater. Des*. **2013**, *49*, 945.
[36] M. Ahmed, T. Li, G. Casillas, J. M. Cairney, D. Wexler, E. V. Pereloma, *J. Alloy Compd*. **2015**, *629*, 260.
[37] H. Matsumoto, M. Kitamura, Y. Li, Y. Koizumi, A. Chiba, *Mater. Sci. Eng. A* **2014**, *611*, 337.